Magnetic order in geometrically frustrated $Gd_2(Ti_{1-x}Zr_x)_2O_7$ ($x = 0.02$ and 0.15) single crystals

Da-qian Liao, M. R. Lees,* D. W. Baker, D. McK. Paul, and G. Balakrishnan
Physics Department, University of Warwick, Coventry, CV4 7AL, UK

(Received 24 August 2010; revised manuscript received 5 November 2010; published 10 February 2011)

Single crystals of $Gd_2(Ti_{1-x}Zr_x)_2O_7$ with $x = 0.02$ and 0.15 have been used to investigate the effects of Zr doping on the properties of the geometrically frustrated antiferromagnet $Gd_2Ti_2O_7$. Powder and single-crystal x-ray data, along with optical birefringence measurements, reveal that the $x = 0.02$ sample retains the cubic $Fd\bar{3}m$ structure of pure $Gd_2Ti_2O_7$, while the $x = 0.15$ composition adopts a tetragonal $I4_1/amd$ structure. Low-temperature magnetization and specific heat measurements show that for $Gd_2(Ti_{0.98}Zr_{0.02})_2O_7$ there are two magnetic transitions at $T_{N1} = 1.02$ K and $T_{N2} = 0.70$ K, but for $Gd_2(Ti_{0.85}Zr_{0.15})_2O_7$ a single transition is observed at $T_N = 1.02$ K. Changes in the specific heat with a magnetic field applied along the [110] and the [111] directions are used to construct the H-T phase diagrams for both samples.

DOI: 10.1103/PhysRevB.83.064403 PACS number(s): 75.30.Kz, 75.50.Ee, 75.40.Cx

I. INTRODUCTION

In recent years, geometrically frustrated magnetic systems have attracted a great deal of attention from both experimentalists and theorists.[1–4] Generally such systems are composed of corner or edge-sharing frustrated units made up of triangles or tetrahedra. The three-dimensional pyrochlore structure is a good example of a system which is composed of corner-sharing tetrahedra and many magnetic systems with this structure exhibit unusual low-temperature properties including spin liquid behavior,[5] spin glass freezing in a chemically ordered system,[6,7] or spin ice behavior.[8,9]

Among the geometrically frustrated rare earth titanium pyrochlore oxides, $Gd_2Ti_2O_7$ holds a unique position as the only compound in which the rare earth ions have a negligible single ion anisotropy. Therefore $Gd_2Ti_2O_7$ is a good approximation to a model system characterized by a Heisenberg antiferromagnetic coupling with dipole-dipole interactions as the leading perturbation.[10,11] The antiferromagnetic ordering of $Gd_2Ti_2O_7$ takes place in two steps.[12,13] Below $T_{N1} \sim 1.02$ K there is a partial ordering of three quarters of the Gd moments with a propagation vector $\mathbf{k} = (\frac{1}{2}, \frac{1}{2}, \frac{1}{2})$. This is followed by a second transition at $T_{N2} \sim 0.7$ K to a state with a multi-k (4-k) structure in which the remaining 1/4 of the spins become weakly ordered.[14,15]

$Gd_2Ti_2O_7$ crystallizes in a cubic pyrochlore ($Fd\bar{3}m$) structure. It is reported that the substitution of isovalent Zr for Ti leads to an increase in the lattice parameter of the system and eventually to a phase transition to a defect fluorite ($Fm\bar{3}m$) structure.[16] There is the possibility that cation disorder, with a short-range fluorite-like structure, coexists with the long-range pyrochlore structure for Ti rich compositions. $Gd_2(Ti_{1-x}Zr_x)_2O_7$ displays a variety of interesting properties that may make it suitable for a number of applications; with increasing Zr content, there is a five orders-of-magnitude increase in the oxygen ion conductivity at 875 K,[17] and an increasing resistance to radiation.[18]

We have prepared a set of single crystals samples of $Gd_2(Ti_{1-x}Zr_x)_2O_7$ ($0 \leqslant x \leqslant 0.15$) to study the effects of Zr doping on the low-temperature magnetic properties of this system. In particular, we are interested in how small perturbations to the structure, without disturbing the Gd sublattice, can influence the magnetic order in this system. We present the results of structural characterization studies, and magnetization and specific heat measurements on $Gd_2(Ti_{1-x}Zr_x)_2O_7$ for $x = 0.02$ and 0.15 with a magnetic field applied along either the [110] or the [111] direction. We show that T_{N1} is remarkably robust to the effects of Zr doping and remains unchanged at ~1.02 K across the series. In contrast, replacing Ti with Zr suppresses the magnetic transition at T_{N2} in $Gd_2(Ti_{1-x}Zr_x)_2O_7$. We construct the magnetic H-T phase diagrams for both samples and compare our results with those obtained by Petrenko *et al.* for pure $Gd_2Ti_2O_7$ (Ref. 13).

II. EXPERIMENTAL DETAILS

Polycrystalline samples of $Gd_2(Ti_{1-x}Zr_x)_2O_7$ ($x = 0.02$ and 0.15) were prepared by a solid state reaction. High purity powders of Gd_2O_3 ($\geqslant$99.9%), ZrO_2 (99.99%), and TiO_2 (99.99%) were mixed together in stoichiometric ratios and reacted in air at 1300 °C with intermediate grindings. The powders were then isostatically pressed into rods and sintered at 1350 °C in air. High-quality single crystals of $Gd_2(Ti_{1-x}Zr_x)_2O_7$ were then grown in air using the floating-zone method in an infrared image furnace.[19]

Powder x-ray diffraction spectra were recorded on a Panalytical X'Pert Pro multipurpose x-ray diffraction system in Bragg-Brentano geometry, with a curved Johansson monochromator providing focused CuKα1 radiation. An X'Celerator area detector was used. Rietveld refinements were performed with the TOPAS ACADEMIC refinement program. Single-crystal x-ray diffraction was performed on an Oxford Diffraction Gemini R CCD diffractometer with MoKα radiation.

X-ray diffraction Laue photographs taken using a Philips x-ray generator equipped with a MoKα source and a Photonic-Science camera were used to align the samples.

Optical birefringence measurements on small pieces of the single crystals were made using the rotating-polarizer method with an Oxford Cryosystems Metripol setup, at a wavelength of 550 nm (Ref. 20). The system measures $|\sin\delta|$, where δ is the phase difference introduced in a plane-polarized light wave as it travels through the sample due to a difference Δn in the refractive index n along different crystallographic axes perpendicular to the direction of travel of the light.

Heat capacity measurements were performed in the temperature range 0.05 to 10.0 K in applied magnetic fields H of up to 9 T using a Quantum Design (QD) Physical Property Measurement System calorimeter equipped with both a ^{3}He option and a ^{3}He/^{4}He dilution refrigerator option. Due to the relatively high values of the specific heat of these crystals and the poor thermal conductivity of the materials at low temperature, the heat capacity measurements were restricted to small (mass < 0.5 mg) plate-like samples with a typical thickness of 0.1 mm. Magnetization measurements were made between 0.5 K and room temperature in an applied magnetic field of 0.1 T using a QD Magnetic Properties Measurement System superconducting quantum interference device (SQUID) magnetometer along with an i-Quantum ^{3}He insert.

III. RESULTS

A. High-temperature characterization studies

A small quantity of each of the single crystals was ground into powder. Figure 1 shows the room-temperature x-ray diffraction spectra collected. The data reveal that $Gd_2(Ti_{0.98}Zr_{0.02})_2O_7$ has a cubic structure (space group: $Fd\bar{3}m$) with a lattice parameter $a = 10.200\,79(3)$ Å [cf., $10.193\,73(2)$ Å for pure $Gd_2Ti_2O_7$], so as expected, the addition of Zr leads to an increase in the lattice parameter. In agreement with previous work on $Gd_2Ti_2O_7$ there is no evidence for any mixing of the Gd and Ti/Zr in this material.

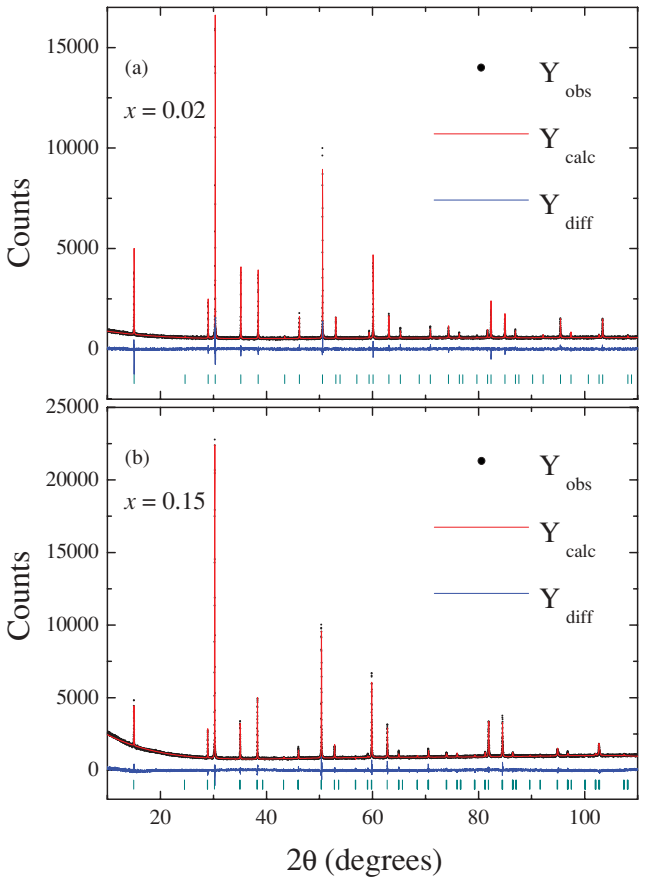

FIG. 1. (Color online) (a) Powder x-ray diffraction pattern of $Gd_2(Ti_{0.98}Zr_{0.02})_2O_7$ together with the profile calculated using the cubic $Fd\bar{3}m$ structure. (b) Powder x-ray diffraction pattern of $Gd_2(Ti_{0.85}Zr_{0.15})_2O_7$ together with the profile calculated using the tetragonal structure $I4_1/amd$ space group. A difference curve is drawn below each data set.

In the spectra of the $x = 0.15$ sample several of the peaks appear broadened. Previously published work has suggested that pure $Gd_2Zr_2O_7$ can, depending on the preparation conditions, form in one of three structures. A "sharp" pyrochlore structure in which there is no mixing of the Gd and Zr atoms within the structure, a "diffuse" pyrochlore structure in which there is some interchange of the Gd and Zr atoms on the 16d and 16c sites, or a fluorite structure.[21] We attempted to fit our powder x-ray data using the two different pyrochlore models. There is no indication from the refinements that any of the Gd sits on the Ti/Zr site since in the refinement using the "diffuse" model, the occupancy of the Gd on the 16c site refines to zero. The "sharp" pyrochlore model gives $a = 10.250\,74(5)$ Å but the overall quality of the fit, as judged by the weighted profile R factor (R_{wp}) and the goodness of fit (GOF), is poor. What is clear from diffraction scans out to 110° in 2θ with a step size of 0.0068°, is that while there is anisotropic broadening of certain peaks, there is also some peak splitting, suggesting that the structure of the $x = 0.15$ sample is, in fact, tetragonal. The $I4_1/amd$ space group was chosen for the tetragonal structure as this is a subgroup of the cubic $Fd\bar{3}m$ structure and allows for a tetragonally distorted pyrochlore structure, where an additional distortion to the oxygen octahedra and tetrahedra are allowed by symmetry. The results of the Rietveld refinement are presented in Table I. The lattice parameters of the cubic structure in the "sharp" pyrochlore model refine to the a and c lattice parameters in the tetragonal model. While the tetragonal model provides a better fit to the data, there is still the issue that some peaks in the spectra are very broad. Preferred orientation corrections were applied in the (00ℓ) direction, but it was found that a spherical harmonic correction was required to fit all of the peaks well.

TABLE I. Refined structural parameters for $Gd_2(Ti_{0.98}Zr_{0.02})_2O_7$ and $Gd_2(Ti_{0.85}Zr_{0.15})_2O_7$. Atom positions for the $Fd\bar{3}m$ (origin choice 2) cubic structure are for Gd, 16d($\frac{1}{2},\frac{1}{2},\frac{1}{2}$); Ti/Zr, 16$c$(0,0,0); O1, 48$f$($x,\frac{1}{8},\frac{1}{8}$); and O2, 8$b$($\frac{3}{8},\frac{3}{8},\frac{3}{8}$), while the atom positions for the $I4_1/amd$ (origin choice 2) tetragonal structure are for Gd, 8d(0,0,$\frac{1}{2}$); Ti/Zr, 8c(0,0,0); O1, 16f(x,$x+\frac{1}{4},\frac{3}{8}$); O2, 4$b$(0,$\frac{1}{4},\frac{5}{8}$); and O3, 8$e$(0,$\frac{3}{4}$,$z$).

	Cubic $x = 0.02$	Cubic $x = 0.15$	Tetragonal $x = 0.15$
Space group	$Fd\bar{3}m$	$Fd\bar{3}m$	$I4_1/amd$
a (Å)	10.200 79(3)	10.250 74(5)	7.250 13(4)
c (Å)			10.2409(1)
Volume (Å^3)	1061.45(1)	1077.13(2)	538.304(9)
O1 x	0.330(1)	0.299(1)	0.699(2)
O3 z			0.034(2)
Z	8	8	4
Refined parameters	27	23	35
Rwp (%)	5.079	5.792	4.592
GOF	1.250	1.883	1.493

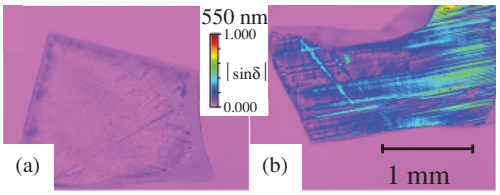

FIG. 2. (Color online) (a) False color images of $|\sin\delta|$ for small sections of single crystals of (a) $Gd_2(Ti_{0.98}Zr_{0.02})_2O_7$ and (b) $Gd_2(Ti_{0.85}Zr_{0.15})_2O_7$ indicating the degree of birefringence within the sample. The samples were polished down to a thickness of $\sim 100\,\mu$m, mounted on glass slides, and images were recorded at room temperature. The pink background results from light passing directly through the glass slide.

Single-crystal data of the $x = 0.15$ sample were also refined in $I4_1/amd$ using SHELX giving a weighted R factor of 4.2%. The fact that no disorder was seen in the data collection for this single crystal further supports the ordered tetragonal structural model over a disordered cubic model.

We also examined the optical anisotropy of the crystals. For the $x = 0.02$ sample [Fig. 2(a)] the data show no evidence for birefringence, indicating that the sample is cubic. There is some evidence for a small degree of strain (indicated by the blue areas) around the perimeter of the sample that may result, in part, from the cutting and polishing procedures performed prior to the measurements. In contrast, for the $x = 0.15$ sample $|\sin\delta|$ is nonzero for large areas of the sample and domains can clearly be seen [Fig. 2(b)]. This confirms that this sample is not cubic.

At $T > 20$ K the dc magnetization versus temperature data (not shown) demonstrate that the samples of $Gd_2(Ti_{1-x}Zr_x)_2O_7$ with $x = 0.02$ and 0.15 are Curie-Weiss paramagnets with Weiss temperatures θ_W that decrease in magnitude very slightly as the Zr content is increased ($\theta_W = -10.14$ K and -9.7 K for $x = 0.02$ and 0.15, respectively). In both samples the Gd^{3+} ions carry the expected effective moment of $7.94\mu_B$.

B. Low-temperature magnetization and heat capacity measurements

Figure 3 shows the temperature dependence of the heat capacity divided by temperature, $C(T)/T$, for single crystals of $Gd_2(Ti_{1-x}Zr_x)_2O_7$ ($x = 0.02$ and 0.15). For $x = 0.02$, two peaks in the specific heat at $T_{N1} = 1.02 \pm 0.02$ K and $T_{N2} = 0.70 \pm 0.02$ K mark consecutive magnetic phase transitions. In contrast to pure $Gd_2Ti_2O_7$, however,[13] the amplitude of the peak at T_{N2} is clearly much smaller than the peak at T_{N1}. At the lowest temperature an upturn in $C(T)/T$ is attributed to electric quadrupole and the nuclear hyperfine interactions of the Gd atoms. For the $x = 0.15$ composition, a single peak in the specific heat at $T_N = 1.02 \pm 0.02$ K is followed by a broad anomaly on the low-temperature side. The upturn in $C(T)/T$ is once again attributed to nuclear contributions from the Gd atoms.

The removal of any indication of the second low-temperature transition in the $x = 0.15$ composition is confirmed by the magnetic susceptibility data. For pure $Gd_2Ti_2O_7$ two transitions are clearly visible as a peak in $\chi_{d.c}(T)$ at

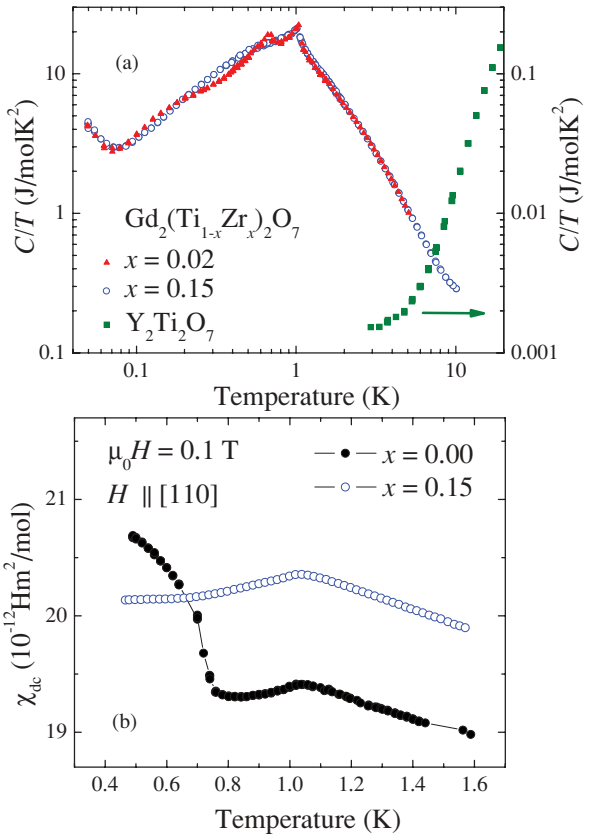

FIG. 3. (Color online) (a) $C(T)/T$ for single crystal samples of $Gd_2(Ti_{1-x}Zr_x)_2O_7$ ($x = 0.02$ and 0.15) and the isostructural non-magnetic compound $Y_2Ti_2O_7$. (b) The low-temperature field-cooled magnetic susceptibility of single crystal samples of $Gd_2(Ti_{1-x}Zr_x)_2O_7$ ($x = 0.00$ and 0.15) with a magnetic field $\mu_0 H = 0.1$ T applied along the [110] direction.

$T_{N1} = 1.02 \pm 0.02$ K and a jump at $T_{N2} = 0.70 \pm 0.05$ K, while for the $x = 0.15$ sample a single peak is seen at $T_N = 1.02 \pm 0.02$ K.

The left-hand panels of Fig. 4 show the temperature dependence of C/T measured in different magnetic fields for a single crystal of $Gd_2(Ti_{0.98}Zr_{0.02})_2O_7$ with $H||[111]$. The application of a magnetic field causes the two peaks present in zero magnetic field to merge leaving a shoulder-like anomaly on the low-temperature side of a single peak at 1.04 K in 0.5 T and, in a field of 1.5 T, a single peak at 0.96 K. As H is increased further, this single peak first shifts to higher temperature before beginning to move to lower temperature. For this field direction a second maximum in the $C(T)/T$ data is also clearly visible at low T in a field of 3 T. For fields above 5 T there are no sharp features in the data and the magnitude of C/T decreases rapidly with increasing H.

The right-hand panels of Fig. 4 show the $C(T)/T$ data for $x = 0.02$ with $H||[110]$. In low fields the behavior is similar to that seen when the field is applied along the [111] direction. The two peaks present in zero field, again merge into a single peak at 0.96 K in 1.5 T. As the applied field is increased further, this single peak is observed at temperatures that are noticeably lower than for $H||[111]$.

We have also measured the magnetic field dependence of the specific heat of $Gd_2(Ti_{0.98}Zr_{0.02})_2O_7$ at fixed temperature for

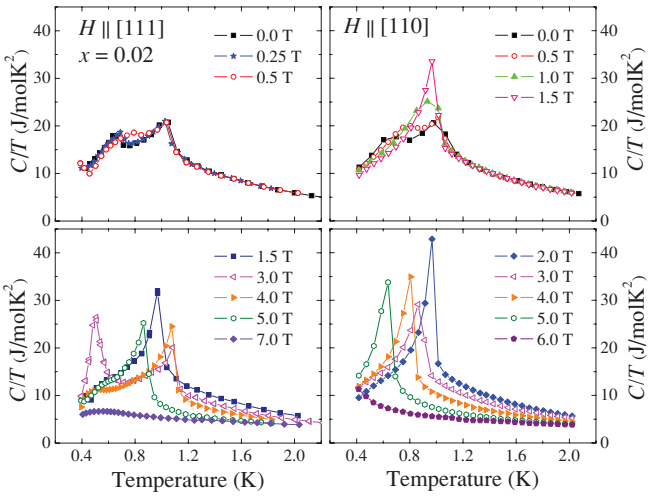

FIG. 4. (Color online) $C(T)/T$ measured on a single crystal of $Gd_2(Ti_{0.98}Zr_{0.02})_2O_7$ in different applied magnetic fields for $H||[111]$ (left) and for $H||[110]$ (right).

$H||[111]$ and $H||[110]$ (see Fig. 5). Two peaks are observed in each $C(H)$ curve. The first peak at lower field occurs at roughly the same point in H-T space for magnetic fields applied along either direction (e.g., 2.6 T at 0.75 K). The second peak in the isothermal data clearly occurs at lower magnetic field when H is applied along the [110], for example, at 0.5 K the peak is at 5.4 T for $H||[110]$ and at 5.8 T for $H||[111]$. Above this second transition, the specific heat decreases with increasing field and at 9 T the magnitude of C/T decreases with decreasing T.

The left-hand panels of Fig. 6 show the H-T magnetic phase diagrams for $x = 0.02$ constructed using the $C(T)$ and $C(H)$ data. For $H||[111]$, the phase diagram is similar to that of pure $Gd_2Ti_2O_7$.[13] At the lowest temperature we observe two phase transitions as the applied field is increased. The first, seen at approximately half the saturation field, is likely to be related to a transition to a collinear spin-state where three of the spins on each tetrahedra are aligned parallel to the applied field, while the fourth lies antiparallel[13,22]. The second phase boundary marks the transition to a saturated paramagnetic phase. Above this phase boundary, the magnetic field along [111] initially favors the onset of magnetic order and the transition temperature is 1.08 K at 4 T (cf., 1.02 K in zero field). For $H||[110]$, the transition to the magnetically ordered state occurs at the same temperatures and magnetic fields as for $H||[111]$, but there is no bulge in the phase diagram around 4 T and the transition to the saturated phase occurs in a lower field.

The left-hand panels of Fig. 7 show the $C(T)/T$ data collected for a single crystal of $Gd_2(Ti_{0.85}Zr_{0.15})_2O_7$ with $H||[111]$. As the magnetic field is increased the single sharp peak in the specific heat at $T_N = 1.02 \pm 0.02$ K shifts monotonically to lower temperature, decreases in magnitude and broadens, before once again sharpening at 5 T. A similar behavior (see Fig. 7) is observed for $H||[110]$ although above 2 T the peak is much broader in temperature and the maximum seen in any particular field is at a lower temperature than the corresponding data for $H||[111]$.

Figure 8 shows the field dependence of the specific heat measured at different temperatures for $x = 0.15$ with $H||[111]$

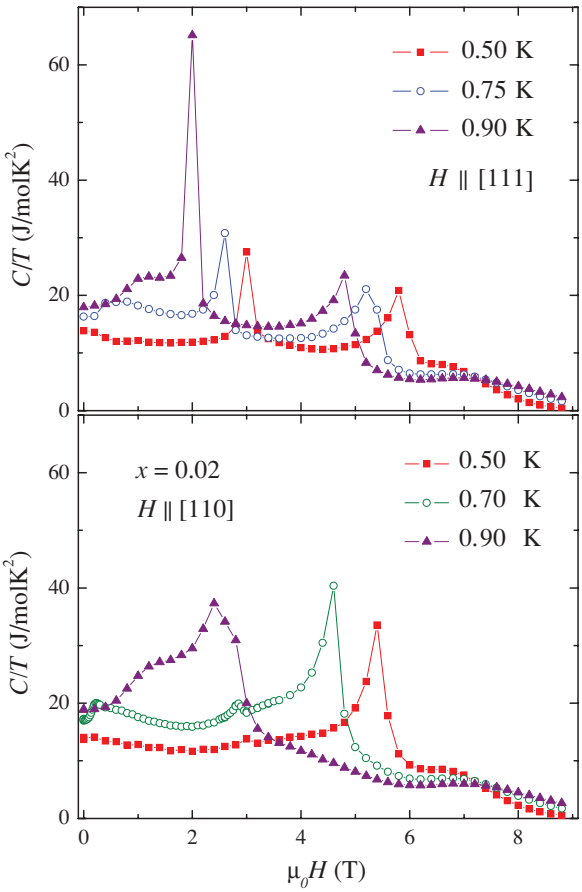

FIG. 5. (Color online) Magnetic field dependence of C/T for a single crystal of $Gd_2(Ti_{0.98}Zr_{0.02})_2O_7$ with a magnetic field applied along either the [111] (upper panel) or the [110] (lower panel) crystallographic directions.

and $H||[110]$. In contrast to the data for the $x = 0.02$ sample, for both magnetic field directions, only one clear maximum is observed in each $C(H)$ curve.

The H-T magnetic phase diagrams for $x = 0.15$ with H applied parallel to [111] and [110] are shown in the right-hand panels of Fig. 6. For both crystallographic directions the applied magnetic field suppresses the magnetic order and the single phase boundary delineates a transition between the (saturated) paramagnetic and a magnetically ordered phase. At the lowest temperatures measured the saturation fields for both crystallographic directions are ∼10% lower than for the $x = 0.02$ sample.

IV. DISCUSSION

We have shown that T_{N1} in $Gd_2(Ti_{1-x}Zr_x)_2O_7$ is remarkably robust to the Zr doping, remaining unchanged at 1.02 K up to $x = 0.15$. This is perhaps not surprising given that for $Gd_2Sn_2O_7$, in which all the Ti is replaced by Sn, T_N is unchanged, although in the Sn compound the magnetic transition becomes first order.[23] We note, however, that $Gd_2Zr_2O_7$ is reported to undergo long-range magnetic order at 0.77 K (Ref. 24) and so doping with as much as 15% Zr may have been expected to have some effect on T_{N1}. In contrast, the second magnetic transition at T_{N2} is quickly removed by

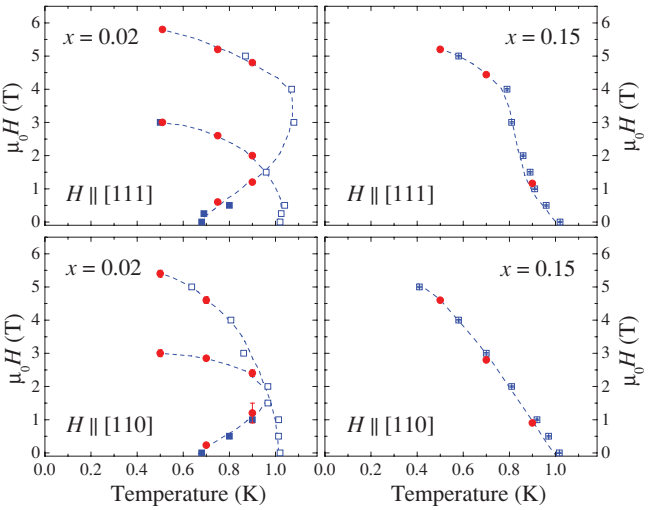

FIG. 6. (Color online) Magnetic H-T phase diagrams for single crystals of $Gd_2(Ti_{0.98}Zr_{0.02})_2O_7$ and $Gd_2(Ti_{0.85}Zr_{0.15})_2O_7$ with a magnetic field applied along the [111] (upper panels) and the [110] (lower panels) crystallographic directions. The open and closed squares are points derived from the $C(T)/T$ data and the closed circles are taken from the $C(H)$ data. The lines connecting the points are a guide to the eye.

the perturbation introduced by the doping with Zr. The Zr doping also modifies the behavior in high magnetic fields, reducing the saturation magnetic field at 0.4 K in the $x = 0.15$ composition by 10% compared to the values seen in the pure[13] and $x = 0.02$ sample at the same temperature. In addition, the degree of anisotropy in the H-T magnetic phase diagram of the $x = 0.15$ is considerably reduced compared to the $x = 0.0$ (Ref. 13) and $x = 0.02$ materials. We note, however, that even for the $x = 0.15$ sample, the application of a magnetic field along the [111] direction still suppresses the onset of magnetic order less rapidly than for magnetic fields applied along [110].

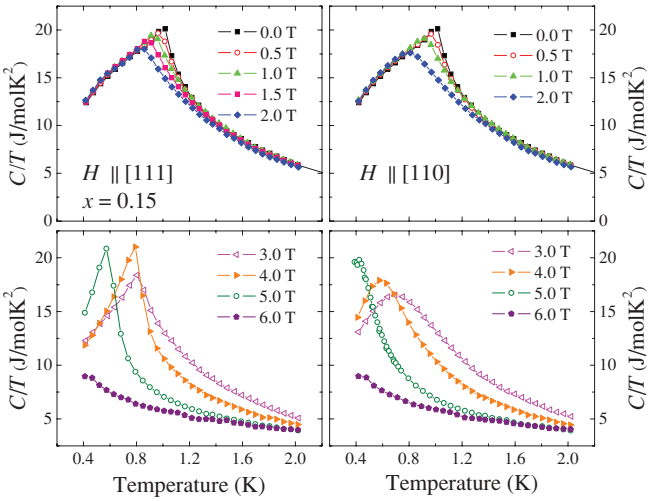

FIG. 7. (Color online) $C(T)/T$ measured on a single crystal of $Gd_2(Ti_{0.85}Zr_{0.15})_2O_7$ in different applied magnetic fields for $H||[111]$ (left) and $H||[110]$ (right).

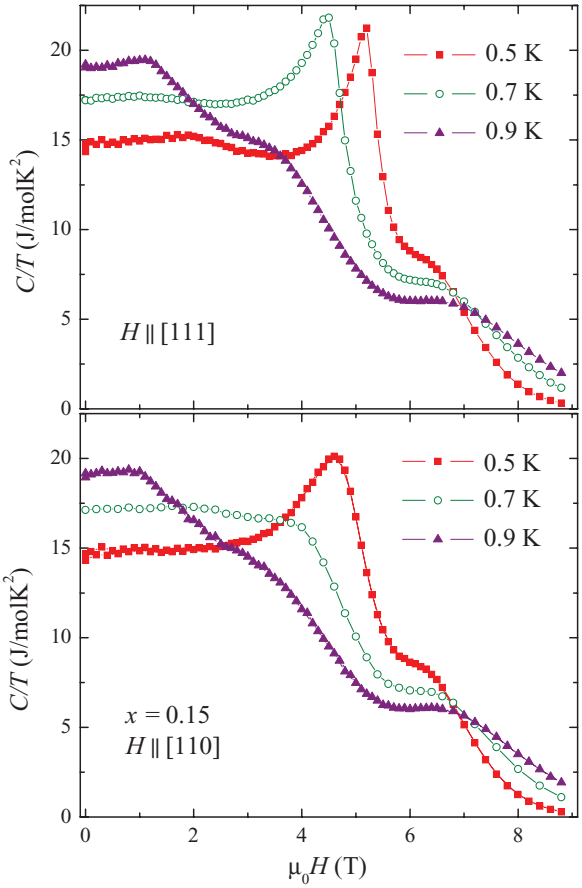

FIG. 8. (Color online) Magnetic field dependence of C/T for a single crystal of $Gd_2(Ti_{0.85}Zr_{0.15})_2O_7$ with a magnetic field applied along either the [111] (upper panel) or the [110] (lower panel) crystallographic directions.

For all the $C(T)$ and $C(H)$ curves presented above, the values of the measured specific heat were identical for increasing and decreasing field and temperature (i.e., no signs of field or temperature history dependence have been detected). This indicates the second-order nature for all the phase transitions in $Gd_2(Ti_{0.98}Zr_{0.02})_2O_7$ and $Gd_2(Ti_{0.85}Zr_{0.15})_2O_7$ in agreement with our earlier observations in $Gd_2Ti_2O_7$ (Ref. 13). The amplitude of the peak in $C(T)$ at T_{N1} (21.5 J/mol K for 2% Zr and 20.4 J/mol K for 15% Zr doping) is also consistent with the mean-field value for a second-order magnetic transition with an $S = 7/2$ magnetic ion (20.4 J/mol K) (Ref. 25).

Using a molecular field model we can estimate the nearest-neighbor exchange interaction J_1 using $J_1 = 3\theta_W/zS(S+1)$ where $z = 6$ is the number of nearest neighbors. Within this framework the small reduction in the magnitude of the Weiss temperature θ_W as the Zr content is increased indicates a weakening of J_1. This could play a role in the removal of the phase transition at T_{N2}. For an isotropic unfrustrated antiferromagnet, a peak in $C(T)$ associated with long-range order is suppressed to zero temperature by a magnetic field $H_c(0) \sim k_B\theta_W/g\mu_B$. The reduction in $|\theta_W|$ may also help to explain the decrease in the saturation field as the Zr content in increased to $x = 0.15$. The increase in the Gd-Gd distance that accompanies the increase in the lattice parameter with Zr

doping should also lead to a reduction in the strength of the dipolar coupling between the Gd moments and perhaps the further nearest-neighbor exchange coupling constants $J_{n\geqslant 2}$. We note, however, that the value of T_{N1} in zero field remains constant up to at least $x = 0.15$ in this series of materials. We therefore suggest that the changes seen in the magnetic behavior at T_{N2} with Zr doping are more likely to be driven by local variations in the strengths of the magnetic interactions rather than any global reduction in the Gd-Gd interaction strength. These local variations will result from the apparent loss of cubic symmetry at $x = 0.15$, as well as any disorder or strain introduced into the sample by the Zr doping, that will, in turn, produce modulations in the interatomic bond lengths and bond angles. We note that earlier work on polycrystalline samples of pure $Gd_2Ti_2O_7$ failed to register the presence of a second magnetic transition at T_{N2} and that this may also be due to a degree of disorder present in the materials studied.[26,27]

The loss of cubic symmetry in $Gd_2(Ti_{0.85}Zr_{0.15})_2O_7$ is rather surprising. The absence of any cation disorder in the samples is consistent with an x-ray photoelectron spectroscopy study of $Gd_2(Ti_{1-x}Zr_x)_2O_7$ that showed that the onset of cation disorder only begins when $x \geqslant 0.25$ (Ref. 28). Nevertheless, low-temperature high-resolution structural studies of pure and doped $Gd_2Ti_2O_7$ are required to clarify the crystallographic structure in these materials, as a reduction in the symmetry may help to explain the nature of the magnetic structure at low temperature in pure $Gd_2Ti_2O_7$[14,15] as well as in these doped materials. Studies of the samples using local probes such as nuclear magnetic resonance and electron microscopy are now underway to better understand what controls the magnetic order in this important class of materials.

The heat capacity in zero magnetic field can be fitted using $C(T) = C_L + C_N + C_m$ where the three terms C_L, C_N, and C_m represent the lattice, the nuclear, and the magnetic contributions to the specific heat, respectively. We assume that the lattice contribution to the specific heat is negligible up to at least 5 K. The total heat capacity of the isostructural compound $Y_2Ti_2O_7$ measured between 2 and 10 K and shown in Fig. 5 reveals that this is a valid assumption.

The nuclear contribution to the specific heat $C_N(T)$ arises from a combination of a nuclear electric quadrupole interaction and a nuclear hyperfine interaction of the Gd atoms. Both ^{155}Gd and ^{157}Gd ($I = 3/2$) carry a nuclear and a quadrupolar moment. Assuming $C_N(T) = AT^{-2}$ we obtain $A \approx 1.75 \times 10^{-4}$ J K/mol Gd for both 2% and 15% Zr doping. These values are in agreement with previous work on $Gd_2Sn_2O_7$ (Ref. 29) and consistent with the values for the hyperfine field of $Gd_2Ti_2O_7$ estimated using Mössbauer spectroscopy.[23]

After subtracting C_N from the total specific heat we can see that the magnetic contribution to C_m at low temperature ($T \leqslant 0.5$ K) varies as T^2 for both the samples. Yaouanc *et al.* reported a T^2 dependence below T_{N2} for the C_m of pure $Gd_2Ti_2O_7$ (Ref. 30). The magnetic component of the heat capacity of $Gd_2Sn_2O_7$ is also reported to show a T^2 dependence immediately below T_N, but with an exponential drop below approximately 350 mK that provides evidence for a gap in the spin-wave excitation spectrum.[23,29] Our measurements made down to lower temperatures than those reported in Refs. 23 and 30 show no evidence for the appearance of a gap in the excitation spectrum of Zr doped $Gd_2Ti_2O_7$. The rather unusual T^2 dependence of C_m is also seen in quasi-two-dimensional spin-glasses[31,32] and in some layered antiferromagnets.[33] Spin-wave theory also predicts a T^2 behavior for two-dimensional antiferromagnets.[34]

To estimate the overall magnetic entropy contained within the specific heat we linearly extrapolate $C_m(T)/T$ from the lowest temperature measured down to 0 K. In 0 T, for both the 2% Zr and 15% Zr samples, just over 35% of the expected entropy $2R\ln(2S+1) = 34.6$ J mol^{-1}K^{-1} is recovered between 0 and T_{N1} while 90% is recovered by 5 K. Data for the 15% Zr sample shows that over 95% of the expected entropy is recovered by 10 K (see Fig. 9). This indicates that in both materials at low temperatures almost the full Gd moment on each corner of the linked tetrahedra orders (or at least freezes) and that short-range magnetic correlations persist in both samples well above T_{N1}.

The two phase diagrams proposed here are consistent with the work of Yip *et al.*[35] who have considered the thermodynamics of bicritical and polycritical points, where at least two or three second-order phase transitions intersect, respectively. The phase diagram for $Gd_2(Ti_{0.98}Zr_{0.02})_2O_7$ contains a polycritical point in which the phase boundaries delineating second-order phase transitions between four different phases meet. Such a polycritical point is thermodynamically allowed. The simple removal of the phase boundary at T_{N2} due the addition of more Zr would leave three second-order transition boundaries meeting at a point. This is thermodynamically forbidden.[35] Given that the transitions from the paramagnetic to the magnetically ordered state appear to remain second order this leaves two possibilities for the $x = 0.15$ composition at low temperature as H is increased. Either a phase transition between two different magnetically ordered phases takes place via a first-order phase transition; we have seen no evidence for such a transition in our data. Or there are no phase transitions in the ordered state, and instead for all temperatures below T_{N1} as the magnetic field is increased, the moments rotate slowly in response to the applied field before entering the saturated

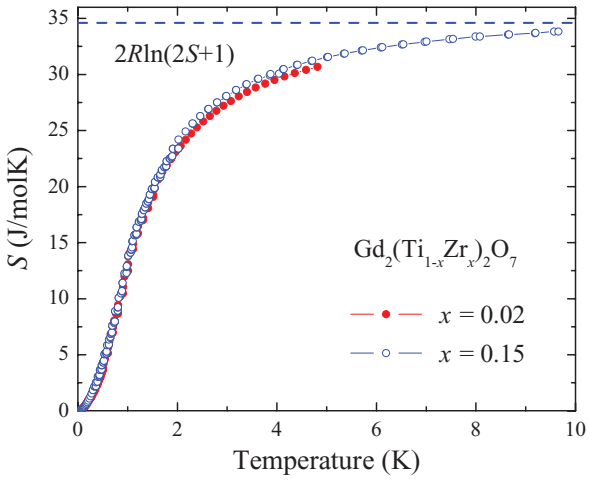

FIG. 9. (Color online) The magnetic entropy S versus temperature for a single crystal of $Gd_2(Ti_{0.98}Zr_{0.02})_2O_7$ and $Gd_2(Ti_{0.85}Zr_{0.15})_2O_7$. The dashed line indicates the expected entropy $2R\ln(2S+1) = 34.6$ J mol^{-1}K^{-1}.

paramagnetic state. This naturally leads us to the simple H-T phase diagram for $Gd_2(Ti_{0.85}Zr_{0.15})_2O_7$ proposed in Fig. 6 .

The description of the H-T phase diagrams presented previously is supported by the observation that for $x = 0.02$ the transition at T_{N1} takes the form of a sharp anomaly for all magnetic fields and for both directions of applied field. This contrasts with the much broader feature seen in $x = 0.15$ data, indicating the entropy associated with the spin moments is released more gradually. For $x = 0.15$, in zero field, we interpret this as an indication that below T_{N1} the system orders with a structure that is similar to that of the $x = 0.02$ sample below T_{N1}, but that the remaining quarter of the magnetic spins freeze at lower temperatures. For the $x = 0.15$ sample, if the magnetic field is then increased within the ordered phase there is a slow rotation of the magnetic moments before the system enters the saturated paramagnetic state.

V. SUMMARY

In summary, we have carried out a detailed study of geometrically frustrated $Gd_2(Ti_{1-x}Zr_x)_2O_7$ ($x = 0.02$ and 0.15) single crystals. In zero magnetic field, two magnetic transitions are observed for $x = 0.02$ while only one transition is observed for $x = 0.15$. Zr doping also leads to dramatic changes in the form of the H-T phase diagrams. On the other hand, both samples still exhibit many common features including a transition to long-range order that occurs at 1.02 K and a low-temperature magnetic contribution to the heat capacity that exhibits a T^2 dependence.

ACKNOWLEDGMENTS

The authors are grateful to O.A. Petrenko and D.S. Keeble for helpful discussions and assistance with the experiments. We acknowledge financial support from the EPSRC, United Kingdom. Some of the equipment used in materials characterization at the University of Warwick was obtained through the Science City Advanced Materials project "Creating and Characterising Next Generation Advanced Material" with support from Advantage West Midlands (AWM) and part funded by the European Regional Development Fund (ERDF).

*m.r.lees@warwick.ac.uk

[1] M. J. Harris and M. P. Zinkin, Mod. Phys. Lett. B **10**, 417 (1996).
[2] P. Schiffer and A. P. Ramirez, Comments Condens. Matter Phys. **18**, 21 (1996).
[3] A. P. Ramirez, Annu. Rev. Mater. Sci. **24**, 453 (1994).
[4] J. S. Gardner, M. J. P. Gingras, and J. E. Greedan, Rev. Mod. Phys. **82**, 53 (2010).
[5] J. S. Gardner, S. R. Dunsiger, B. D. Gaulin, M. J. P. Gingras, J. E. Greedan, R. F. Kiefl, M. D. Lumsden, W. A. MacFarlane, N. P. Raju, J. E. Sonier, I. Swainson, and Z. Tun, Phys. Rev. Lett. **82**, 1012 (1999).
[6] B. D. Gaulin, J. N. Reimers, T. E. Mason, J. E. Greedan, and Z. Tun, Phys. Rev. Lett. **69**, 3244 (1992).
[7] J. S. Gardner, B. D. Gaulin, S.-H. Lee, C. Broholm, N. P. Raju, and J. E. Greedan, Phys. Rev. Lett. **83**, 211 (1999).
[8] M. J. Harris, S. T. Bramwell, D. F. McMorrow, T. Zeiske, and K. W. Godfrey, Phys. Rev. Lett. **79**, 2554 (1997).
[9] A. P. Ramirez, A. Hayashi, R. J. Cava, R. Siddharthan, and B. S. Shastry, Nature (London) **399**, 333 (1999).
[10] S. E. Palmer and J. T. Chalker, Phys. Rev. B **62**, 488 (2000).
[11] J. N. Reimers, A. J. Berlinsky, and A.-C. Shi, Phys. Rev. B **43**, 865 (1991).
[12] A. P. Ramirez, B. S. Shastry, A. Hayashi, J. J. Krajewski, D. A. Huse, and R. J. Cava, Phys. Rev. Lett. **89**, 067202 (2002).
[13] O. A. Petrenko, M. R. Lees, G. Balakrishnan, and D. M. Paul, Phys. Rev. B **70**, 012402 (2004).
[14] J. D. M. Champion, A. S. Wills, T. Fennell, S. T. Bramwell, J. S. Gardner, and M. A. Green, Phys. Rev. B **64**, 140407 (2001).
[15] J. R. Stewart, G. Ehlers, A. S. Wills, S. T. Bramwell, and J. S. Gardner, J. Phys. Condens. Matter **16**, L321 (2004).
[16] N. J. Hess, B. D. Begg, S. D. Conradson, D. E. McCready, P. L. Gassman, and W. J. Weber, J. Phys. Chem. B **106**, 4663 (2002).
[17] H. L. Tuller and P. K. Moon, Mater. Sci. Eng. B **1**, 171 (1988).
[18] W. J. Weber and R. C. Ewing, Science **289**, 2051 (2000).
[19] G. Balakrishnan, O. A. Petrenko, M. R. Lees, and D. M. Paul, J. Phys. Condens. Matter **10**, L723 (1998).
[20] I. G. Wood and A. M. Glazer, J. Appl. Crystallogr. **13**, 217 (1980).
[21] T. Moriga, A. Yoshiasa, F. Kanamaru, K. Koto, M. Yoshimura, and S. Smiya, Solid State Ionics **31**, 319 (1989).
[22] M. E. Zhitomirsky, A. Honecker, and O. A. Petrenko, Phys. Rev. Lett. **85**, 3269 (2000).
[23] P. Bonville, J. A. Hodges, M. Ocio, J. P. Sanchez, P. Vulliet, S. Sosin, and D. Braithwaite, J. Phys. Condens. Matter **15**, 7777 (2003).
[24] A. M. Durand, P. Klavins, and L. R. Corruccini, J. Phys. Condens. Matter **20**, 235208 (2008).
[25] H. E. Stanley, *Introduction to Phase Transitions and Critical Phenomena* (Clarendon, Oxford, 1971).
[26] N. P. Raju, M. Dion, M. J. P. Gingras, T. E. Mason, and J. E. Greedan, Phys. Rev. B **59**, 14489 (1999).
[27] S. R. Dunsiger, R. F. Kiefl, J. A. Chakhalian, J. E. Greedan, W. A. MacFarlane, R. I. Miller, G. D. Morris, A. N. Price, N. P. Raju, and J. E. Sonier, Phys. Rev. B **73**, 172418 (2006).
[28] J. Chen, J. Lian, L. M. Wang, R. C. Ewing, R. G. Wang, and W. Pan, Phys. Rev. Lett. **88**, 105901 (2002).
[29] J. A. Quilliam, K. A. Ross, A. G. Del Maestro, M. J. P. Gingras, L. R. Corruccini, and J. B. Kycia, Phys. Rev. Lett. **99**, 097201 (2007).
[30] A. Yaouanc, P. Dalmas de Réotier, V. Glazkov, C. Marin, P. Bonville, J. A. Hodges, P. C. M. Gubbens, S. Sakarya, and C. Baines, Phys. Rev. Lett. **95**, 047203 (2005).
[31] A. P. Ramirez, G. P. Espinosa, and A. S. Cooper, Phys. Rev. Lett. **64**, 2070 (1990).
[32] A. P. Ramirez, B. Hessen, and M. Winklemann, Phys. Rev. Lett. **84**, 2957 (2000).
[33] B. F. Woodfield, M. L. Wilson, and J. M. Byers, Phys. Rev. Lett. **78**, 3201 (1997).
[34] R. Kubo, Phys. Rev. **87**, 568 (1952).
[35] S. K. Yip, T. Li, and P. Kumar, Phys. Rev. B **43**, 2742 (1991).